Eur. Phys. J. C 12, 77–86 (2000)
Digital Object Identifier (DOI) 10.1007/s100529900202

THE EUROPEAN PHYSICAL JOURNAL C

The hard bremsstrahlung correction to $e^+e^- \to 4f$ with finite fermion masses: results for $e^+e^- \to u\bar{d}\mu^-\bar{\nu}_\mu$ ⋆

F. Jegerlehner[1], K. Kołodziej[2]

[1] Deutsches Elektronen-Synchrotron DESY, Platanenallee 6, 15768 Zeuthen, Germany
[2] Institute of Physics, University of Silesia, ul. Uniwersytecka 4, 40007 Katowice, Poland

Received: 5 July 1999 / Published online: 16 November 1999

Abstract. An improved efficient method of calculating the hard bremsstrahlung correction to $e^+e^- \to 4f$ for non-zero fermion masses is presented. The non-vanishing fermion masses allow us to perform the phase space integrations to the very collinear limit. We therefore can calculate cross sections independent of angular cuts. Such calculations are important for background studies. Results are presented for the total and some differential cross sections for $e^+e^- \to u\bar{d}\mu^-\bar{\nu}_\mu$ and the corresponding hard bremsstrahlung process. The latter is of particular interest for a detailed investigation of the effects of final state radiation. In principle, the process $e^+e^- \to u\bar{d}\mu^-\bar{\nu}_\mu\gamma$ is also interesting since it helps to set bounds on possible anomalous triple and quartic gauge boson couplings involving photons. The size of mass effects is illustrated by comparing the final states $u\bar{d}\mu^-\bar{\nu}_\mu(\gamma)$, $c\bar{s}\mu^-\bar{\nu}_\mu(\gamma)$ and $u\bar{d}\tau^-\bar{\nu}_\tau(\gamma)$.

1 Introduction

Precision measurements of properties of the intermediate gauge bosons Z and W have deepened our understanding of the electroweak interactions and consolidated the validity of the electroweak Standard Model (SM) considerably in the past decade. After the convincing success of LEP1 and SLD experiments in pinning down the properties of the Z resonance we expect further advances in measurements of the properties of the W boson which are not yet known with comparable precision. As the SM very precisely predicts the mass and the width of the W a high accuracy determination of these parameters is of crucial importance, because they allow us to improve indirect bounds on the Higgs mass or on new physics beyond the SM. The precision of ongoing measurements, single W production at the hadron collider TEVATRON, and W pair production at LEP2 are limited by statistics and/or by lack of detailed theoretical understanding.

The proper analysis of $W^\pm$ pair production at LEP2 and later at future high energy e^+e^- linear colliders requires the accurate knowledge of the SM predictions including all relevant radiative corrections. What we need is a detailed understanding of the production and subsequent decay of W pairs, including the background processes and photon radiation: $e^+e^- \to 4f, 4f\gamma, 4f\gamma\gamma, \cdots$, where $4f$ denotes a possible four fermion final state. The lowest order theoretical results for all the possible four fermion final states have been already implemented in several Monte Carlo event generators and semi-analytic programs, which have been thoroughly compared in [1]. Most of the programs include some classes of radiative corrections such as the initial and final state radiation, Coulomb corrections, running of the fine structure constant, etc. While presently available $e^+e^- \to 4f, 4f\gamma$ matrix elements are precise enough for the analysis of LEP2 data [2], at future linear colliders, a much better knowledge of the radiative corrections will be necessary because of the high statistics expected at these accelerators and because radiative corrections get more significant at higher energies.

The complete one-loop electroweak radiative corrections to the on-shell $W^\pm$ pair production including soft bremsstrahlung were calculated in [3]. The hard bremsstrahlung process $e^+e^- \to W^+W^-\gamma$ was included in [4] and [5]. For the process $e^+e^- \to W^+W^- \to 4f$ of actual interest to the experiments only partial results are available. We refer to [6] for a recent review of the status of precision calculations for this case.

Sufficiently above the $W^\pm$ pair production threshold, for most of the present applications, it seems to be sufficient to take into account corrections to the double-resonant diagrams only, i.e., $e^+e^- \to 4f$ via virtual W^+W^- intermediate states. The validity of this approximation has to be controlled by more complete calculations, however. From a theoretical point of view it is certainly necessary to evaluate the complete $O(\alpha)$ radiative corrections for the different channels of the $2 \to 4$ fermion reactions. However, despite of the fact that some progress in calculating the complete virtual one-loop electroweak radiative corrections to $e^+e^- \to u\bar{d}\mu^-\bar{\nu}_\mu$ have been reported in [7], the

⋆ Work supported in part by the Polish State Committee for Scientific Research (KBN) under contract number 2 P03B 033 14.

final result of such a calculation is still missing. Concerning the real photon emission, the situation looks much better. The hard bremsstrahlung for four fermion reactions mediated by two resonant W bosons was calculated in [8]. A similar calculation, extended by an inclusion of collinear effects, was presented as a package WWF [9]. The complete lowest order result for $e^+e^- \to e^-\bar{\nu}_e u\bar{d}\gamma$ was presented in [10] and calculations of $e^+e^- \to 4f\gamma$ for an arbitrary final state were reported in [11]. Results on bremsstrahlung for purely leptonic reactions have been published in [6] and most recently predictions for all processes $e^+e^- \to 4f\gamma$ with massless fermions have been presented in [12].

At a future linear collider, the proper treatment of the collinear photons will be crucial and it requires to take into account the fermion masses appropriately. Therefore, in the present paper, we propose an efficient method of calculating the hard photon bremsstrahlung for four fermion production in e^+e^- annihilation without neglecting the fermion masses. The phase space integration can therefore be performed to the very collinear limit. This allows for calculating cross sections independent of angular cuts and estimating background contributions coming from undetected hard photons. We present results for the total and a few differential cross sections for the channel $e^+e^- \to u\bar{d}\mu^-\bar{\nu}_\mu$ and the corresponding bremsstrahlung process. The latter is particularly suited for a detailed investigation of effects related to final state photon emission, since the muons appear well separated from photons in the detectors. In particular, it seems to be interesting to study the influence of final state radiation on the W mass measurement via this channel. Having the final state photon resolution in $e^+e^- \to u\bar{d}\mu^-\bar{\nu}_\mu\gamma$ could also make it possible to investigate the quartic γVWW couplings ($V = \gamma, Z$), which are absent on the Born level of $4f$ production. Of course, besides the new quartic couplings there are additional triple γWW vertices as well. In the soft photon limit, we can perform the integration over the soft photon phase space analytically and demonstrate the cut-off independence of the combined soft and hard photon bremsstrahlung cross section. We finally will illustrate the importance of mass effects by comparing the channels where $u\bar{d}$ is replaced by $c\bar{s}$. Similarly, we may replace the μ by a τ lepton.

2 Method of calculation

In this section, we present a method for calculating the matrix elements of a two-fermion to four fermion reaction and an associated bremsstrahlung photon. The method is an extension of the helicity amplitude method introduced in [4] to final states of arbitrary spin.

As in [4], we use the Weyl representation for fermions where the Dirac matrices $\gamma^\mu, \mu = 0, 1, 2, 3$, are given in terms of the unit 2×2 matrix I and Pauli matrices $\sigma_i, i = 1, 2, 3$, by

$$\gamma^\mu = \begin{pmatrix} 0 & \sigma_+^\mu \\ \sigma_-^\mu & 0 \end{pmatrix}, \tag{1}$$

with $\sigma_\pm^\mu = (I, \pm\sigma_i)$. In representation (1), the matrix $\gamma_5 = \mathrm{i}\gamma^0\gamma^1\gamma^2\gamma^3$ and the chiral projectors $P_\pm = (1 \pm \gamma_5)/2$ read

$$\gamma_5 = \begin{pmatrix} -I & 0 \\ 0 & I \end{pmatrix}, \quad P_- = \begin{pmatrix} I & 0 \\ 0 & 0 \end{pmatrix}, \quad P_+ = \begin{pmatrix} 0 & 0 \\ 0 & I \end{pmatrix}. \tag{2}$$

A contraction of any four-vector a^μ with the γ^μ matrices of (1) has the form

$$\not{a} = a^\mu\gamma_\mu = \begin{pmatrix} 0 & a^\mu\sigma_\mu^+ \\ a^\mu\sigma_\mu^- & 0 \end{pmatrix} = \begin{pmatrix} 0 & a^+ \\ a^- & 0 \end{pmatrix}. \tag{3}$$

The 2×2 matrices $a^\pm$ can be expressed in terms of the components of the four-vector a^μ by

$$\begin{aligned} a^+ &= \begin{pmatrix} a^0 - a^3 & -a^1 + \mathrm{i}a^2 \\ -a^1 - \mathrm{i}a^2 & a^0 + a^3 \end{pmatrix}, \\ a^- &= \begin{pmatrix} a^0 + a^3 & a^1 - \mathrm{i}a^2 \\ a^1 + \mathrm{i}a^2 & a^0 - a^3 \end{pmatrix}. \end{aligned} \tag{4}$$

In representation (1), the helicity spinors for a particle, $u(\boldsymbol{p}, \lambda)$, and an antiparticle, $v(\boldsymbol{p}, \lambda)$, of four-momentum $(E, \boldsymbol{p})$ and helicity $\lambda/2 = \pm 1/2$ are given by

$$\begin{aligned} u(\boldsymbol{p}, \lambda) &= \begin{pmatrix} \sqrt{E - \lambda|\boldsymbol{p}|}\chi(\boldsymbol{p}, \lambda) \\ \sqrt{E + \lambda|\boldsymbol{p}|}\chi(\boldsymbol{p}, \lambda) \end{pmatrix}, \\ v(\boldsymbol{p}, \lambda) &= \begin{pmatrix} -\lambda\sqrt{E + \lambda|\boldsymbol{p}|}\chi(\boldsymbol{p}, -\lambda) \\ \lambda\sqrt{E - \lambda|\boldsymbol{p}|}\chi(\boldsymbol{p}, -\lambda) \end{pmatrix}, \end{aligned} \tag{5}$$

and the helicity eigenstates $\chi(\boldsymbol{p}, \lambda)$ can be expressed in terms of the spherical angles θ and ϕ of the momentum vector $\boldsymbol{p}$ as[1]

$$\begin{aligned} \chi(\boldsymbol{p}, +1) &= \begin{pmatrix} \cos\theta/2 \\ \mathrm{e}^{\mathrm{i}\phi}\sin\theta/2 \end{pmatrix}, \\ \chi(\boldsymbol{p}, -1) &= \begin{pmatrix} -\mathrm{e}^{-\mathrm{i}\phi}\sin\theta/2 \\ \cos\theta/2 \end{pmatrix}. \end{aligned} \tag{6}$$

For simplicity we use real polarization vectors which are defined again in terms of θ and ϕ

$$\begin{aligned} \varepsilon^\mu(\boldsymbol{p}, 1) &= (0, \cos\theta\cos\phi, \cos\theta\sin\phi, -\sin\theta), \\ \varepsilon^\mu(\boldsymbol{p}, 2) &= (0, -\sin\phi, \cos\phi, 0) \end{aligned} \tag{7}$$

$$\varepsilon^\mu(\boldsymbol{p}, 3) = \gamma(\beta, \sin\theta\cos\phi, \sin\theta\sin\phi, \cos\theta), \tag{8}$$

where the longitudinal polarization component of (8) is defined exclusively for a massive vector particle of energy $m\gamma$ and momentum $m\gamma\beta$. We could use complex polarization vectors in the helicity basis as well, if we were interested in definite helicity polarizations.

A polarized matrix element is calculated for a given set of external particle momenta in a fixed reference frame,

[1] Note that our phase convention differs from the one chosen in [4].

e.g. the center of mass system (c.m.s.) of the initial particles, where the initial momenta are parallel to the z axis.

Fermion masses are kept nonzero. The mass effects play an essential role in the bremsstrahlung reactions whenever a collinear photon is emitted. They also are important for tree level reactions with identical particles in the initial and final state, where a photon exchanged in the t channel approaches its mass-shell. Moreover, by keeping the fermion masses finite the Higgs boson exchange can be incorporated in a consistent way.

In order to speed up numerical computation, we decompose the Feynman graphs into factors which depend on a single uncontracted vector index and therefore may be considered as generalized polarization vectors. They can be easily computed and used as building blocks of other graphs. For example, the coupling of an internal gauge boson to the external fermions may be considered as the generalized polarization vector ε_V^μ which is defined as

$$\begin{aligned}\varepsilon_V^\mu(p_1,p_2,\lambda_1,\lambda_2) &= D_V^{\mu\nu}(q)\bar\psi_1(p_1,\lambda_1)\gamma_\nu \\ &\times\left(g_V^{(-)}P_- + g_V^{(+)}P_+\right)\psi_2(p_2,\lambda_2) \\ &= \Big[-\left(g_V^{(+)}\bar\psi_1^I\sigma_+^\mu\psi_2^{II} + g_V^{(-)}\bar\psi_1^{II}\sigma_-^\mu\psi_2^I\right) \\ &+q^\mu/M_V^2\left(\left(m_1g_V^{(-)} - m_2g_V^{(+)}\right)\bar\psi_1^I\psi_2^I\right. \\ &+\left.\left(m_1g_V^{(+)} - m_2g_V^{(-)}\right)\bar\psi_1^{II}\psi_2^{II}\right)\Big]/\left(q^2-M_V^2\right) \quad (9)\end{aligned}$$

where $\bar\psi_1(p_1,\lambda_1) = (\bar\psi_1^I, \bar\psi_1^{II})$ and $\psi_2(p_2,\lambda_2) = (\psi_2^I, \psi_2^{II})$ are spinors for a particle or an antiparticle of four-momentum p_i, mass m_i and helicity λ_i, as defined in (5). We have denoted the chiral couplings of the $\bar\psi_1\psi_2V$ vertex by $g_V^{(\pm)}$, $D_V^{\mu\nu}(q)$ is the photon propagator in the Feynman gauge or the massive gauge boson propagator in the unitary gauge and $q = \pm p_1 \pm p_2$ is the four-momentum transfer. The $+(-)$ sign corresponds to an outgoing (incoming) particle. In the case of a photon propagator we have $M_V = 0$ and only the first term in the square brackets on the right hand side of (9) is present.

The photon emission from any of the external fermion legs of the $\bar\psi_1\psi_2V$ vertex can be taken into account by defining two other generalized polarization vectors:

$$\begin{aligned}\varepsilon_{\gamma V}^\mu(p_1,p_2,k,\lambda_1,\lambda_2,\lambda) &= D_V^{\mu\nu}(q+k)\bar\psi_1(p_1,\lambda_1)g_{\gamma1}\not\varepsilon(k,\lambda) \\ &\times\frac{\pm\not p_1 + \not k + m_1}{(\pm p_1+k)^2-m_1^2}\gamma_\nu\left(g_V^{(-)}P_- + g_V^{(+)}P_+\right)\psi_2(p_2,\lambda_2) \\ &= \frac{g_{\gamma1}}{2p_1\cdot k}D_V^{\mu\nu}(q+k)\Big[g_V^{(+)}\bar\psi_1^I\left(2p_1\cdot\varepsilon \mp k^+\varepsilon^-\right)\sigma_\nu^+\psi_2^{II} \\ &+g_V^{(-)}\bar\psi_1^{II}\left(2p_1\cdot\varepsilon \mp k^-\varepsilon^+\right)\sigma_\nu^-\psi_2^I\Big], \quad (10)\end{aligned}$$

where the upper (lower) sign is assumed if ψ_1 represents an outgoing particle (incoming antiparticle) and

$$\begin{aligned}\varepsilon_{V\gamma}^\mu(p_1,p_2,k,\lambda_1,\lambda_2,\lambda) &= D_V^{\mu\nu}(q+k)\bar\psi_1(p_1,\lambda_1)\gamma_\nu \\ &\times\left(g_V^{(-)}P_- + g_V^{(+)}P_+\right)\frac{\pm\not p_2 - \not k + m_2}{(\pm p_2-k)^2-m_2^2} \\ &\times g_{\gamma2}\not\varepsilon(k,\lambda)\psi_2(p_2,\lambda_2) \\ &= \frac{g_{\gamma2}}{2p_2\cdot k}D_V^{\mu\nu}(q+k)\Big[g_V^{(+)}\bar\psi_1^I\sigma_\nu^+\left(-2p_2\cdot\varepsilon \pm k^-\varepsilon^+\right)\psi_2^{II} \\ &+g_V^{(-)}\bar\psi_1^{II}\sigma_\nu^-\left(-2p_2\cdot\varepsilon \pm k^+\varepsilon^-\right)\psi_2^I\Big], \quad (11)\end{aligned}$$

where the upper (lower) sign has to be taken when ψ_2 represents an incoming particle (outgoing antiparticle). In (10) and (11), $\varepsilon^\mu(k,\lambda)$ is the photon polarization vector as defined in (7) and $g_{\gamma i}$ are the photon couplings to ψ_i.

If we contract the triple gauge boson coupling

$$\begin{aligned}\Gamma_{(WWV)}^{\mu\nu\rho}(p_1,p_2,p_3) &= g_{WWV}\left[(p_1-p_2)^\rho g^{\mu\nu}\right. \quad (12)\\ &+\left.(p_2-p_3)^\mu g^{\nu\rho} + (p_3-p_1)^\nu g^{\mu\rho}\right],\end{aligned}$$

where p_1, p_2 and p_3 are the incoming momenta of the W_μ^+, W_ν^- and the neutral gauge boson V_ρ, $V = \gamma, Z^0$, respectively, with two (generalized) polarization vectors, say ε_1^ν, ε_2^ρ, and with a gauge boson propagator we will obtain another generalized polarization vector, e.g.

$$\varepsilon_V^\sigma(1,2) = D_V^{\sigma\mu}(q)\Gamma_{\mu\nu\rho}^{(WWV)}\varepsilon_1^\nu\varepsilon_2^\rho. \quad (13)$$

In (13), 1 and 2 stay for the four-momenta and polarizations. With the help of the generalized polarization vectors (9–11) and (13), the amplitude corresponding to any Feynman diagram of a process $e^+e^- \to 4f(\gamma)$ may be represented by one of the scalar functions F_{2n+1}, E_3 or E_4 we are going to define now. A fermion line containing $n+1$ couplings to gauge bosons and n fermion propagators sandwiched between external spinors can be represented by the scalar function

$$\begin{aligned}&F_{2n+1}\left(\bar\psi_1, g_1^{(+)}\varepsilon_1^+, g_1^{(-)}\varepsilon_1^-, p_1^+, p_1^-, m_1, g_2^{(+)}\varepsilon_2^+, g_2^{(-)}\varepsilon_2^-, p_2^+,\right. \\ &\left. p_2^-, m_2, \cdots, p_n^+, p_n^-, m_n, g_{n+1}^{(+)}\varepsilon_{n+1}^+, g_{n+1}^{(-)}\varepsilon_{n+1}^-, \psi_2\right) \quad (14)\\ &= \bar\psi_1\not\varepsilon_1\left(g_1^{(-)}P_- + g_1^{(+)}P_+\right)\tfrac{\not p_1+m_1}{p_1^2-m_1^2}\not\varepsilon_2\left(g_2^{(-)}P_-\right. \\ &\left.+g_2^{(+)}P_+\right)\tfrac{\not p_2+m_2}{p_2^2-m_2^2}\cdots\tfrac{\not p_n+m_n}{p_n^2-m_n^2}\not\varepsilon_{n+1}\left(g_{n+1}^{(-)}P_- + g_{n+1}^{(+)}P_+\right)\psi_2,\end{aligned}$$

where we have suppressed polarization indices. In the representation (1–5), the algebra of 4×4 matrices in (14) can be easily reduced to the algebra of 2×2 matrices. This kind of reduction has been used already in (9–11). Utilizing the 2×2 algebraic representation speeds up the numerical computation and allows for a simultaneous calculation of the γ and Z contributions. We have indicated the use of the reduced form by writing explicitly the dependence on the 2×2 matrices $\varepsilon_i^\pm, p_i^\pm$, defined according to (4), on the left hand side of (14). The general form of this reduction is quite a complicated formula. Therefore, we restrict ourselves to the presentation of an example of the function F_3 which can be written as

$$\begin{aligned}&F_3\left(\bar\psi_1, g_1^{(+)}\varepsilon_1^+, g_1^{(-)}\varepsilon_1^-, p_1^+, p_1^-, m_1, g_2^{(+)}\varepsilon_2^+, g_2^{(-)}\varepsilon_2^-\right) \\ &= m_1g_1^{(+)}g_2^{(-)}\bar\psi_1^I\varepsilon_1^+\varepsilon_2^-\psi_2^I + g_1^{(+)}g_2^{(+)}\bar\psi_1^I\varepsilon_1^+p_1^-\varepsilon_2^+\psi_2^{II} \quad (15)\\ &+g_1^{(-)}g_2^{(-)}\bar\psi_1^{II}\varepsilon_1^-p_1^+\varepsilon_2^-\psi_2^I + m_1g_1^{(-)}g_2^{(+)}\bar\psi_1^{II}\varepsilon_1^-\varepsilon_2^+\psi_2^{II}.\end{aligned}$$

A contraction of the triple gauge boson coupling (12) with three polarization vectors $\varepsilon_1^\mu, \varepsilon_2^\nu$ and ε_3^ρ can be considered

as a scalar function

$$E_3\,[p_1,\varepsilon_1,p_2,\varepsilon_2,p_3,\varepsilon_3) = g_{WWV}\,((p_1-p_2)\cdot\varepsilon_3\varepsilon_1\cdot\varepsilon_2 + (p_2-p_3)\cdot\varepsilon_1\varepsilon_2\cdot\varepsilon_3 + (p_3-p_1)\cdot\varepsilon_2\varepsilon_1\cdot\varepsilon_3]\,. \quad (16)$$

Similarly, the quartic gauge boson coupling

$$\Gamma^{\mu\nu\rho\sigma}_{(4)} = g_{V_1V_2WW}\,(g^{\mu\rho}g^{\nu\sigma} + g^{\mu\sigma}g^{\nu\rho} - 2g^{\mu\nu}g^{\rho\sigma})\,, \quad (17)$$

where the vector indices μ,ν are associated with the neutral gauge bosons V_1 and V_2 and ρ,σ with W^+ and W^-, if contracted with four polarization vectors $\varepsilon_1^\mu,\varepsilon_2^\nu,\varepsilon_3^\rho$ and ε_4^σ can be considered as another scalar function

$$E_4\,(\varepsilon_1,\varepsilon_2,\varepsilon_3,\varepsilon_4) = g_{V_1V_2WW}\,(\varepsilon_1\cdot\varepsilon_3\varepsilon_2\cdot\varepsilon_4 + \varepsilon_1\cdot\varepsilon_4\varepsilon_2\cdot\varepsilon_3 - 2\varepsilon_1\cdot\varepsilon_2\varepsilon_3\cdot\varepsilon_4)\,. \quad (18)$$

Note that similar scalar functions can be defined for the Higgs boson by replacing the vector boson coupling and propagator in (9–11) and (13) by the Higgs coupling and propagator.

The functions (14), (16) and (18) can easily be implemented in a Fortran program and may be computed numerically for any specific set of the particle momenta and polarizations. The Fortran 90 language standard which contains a number of new features and intrinsic functions especially for array manipulations is particularly suitable for this task.

The method described above can be used to calculate the matrix element of any process of e^+e^- annihilation into four fermions and a photon. Actually, the method is quite general and can be applied to any $2 \to n$ tree level reaction, not necessarily in the framework of the standard model, with massive or massless fermions and/or bosons in the final state. However, it may happen that one or a few extra functions will have to be defined in addition to those defined in (14), (16) and (18). Practically the only limitation of the method is the feasibility of phase space integration which is performed numerically by applying the Monte Carlo method.

3 Application to $e^+e^- \to u\bar{d}\mu^-\bar{\nu}_\mu$ and $e^+e^- \to u\bar{d}\mu^-\bar{\nu}_\mu\gamma$

Let us demonstrate how the method of Sect. 2 works in case of the tree level four fermion reaction

$$e^+(p_1,\lambda_1) + e^-(p_2,\lambda_2) \to u(p_3,\lambda_3) + \bar{d}(p_4,\lambda_4) + \mu^-(p_5,\lambda_5) + \bar{\nu}_\mu(p_6,\lambda_6), \quad (19)$$

where the four-momenta and helicities are indicated in parenthesis. The Feynman diagrams of the process (19) are shown in Fig. 1. Although the fermion mass effects are irrelevant for the reaction (19), we keep masses finite for the sake of illustration. However, we neglect the Higgs boson exchange contribution which is suppressed by ratios of the fermion masses to the W boson mass.

We define the necessary generalized polarization vectors using (9):

$$\begin{aligned}
\varepsilon^\mu_\gamma(p_1,p_2,\lambda_1,\lambda_2) &= D^{\mu\nu}_\gamma(p_{12})\bar{v}_1(p_1,\lambda_1)\gamma_\nu g_{\gamma e}u_2(p_2,\lambda_2),\\
\varepsilon^\mu_Z(p_1,p_2,\lambda_1,\lambda_2) &= D^{\mu\nu}_Z(p_{12})\bar{v}_1(p_1,\lambda_1)\gamma_\nu\\
&\quad\times\left(g^{(-)}_{Ze}P_- + g^{(+)}_{Ze}P_+\right)u_2(p_2,\lambda_2),\\
\varepsilon^\mu_{W^+}(p_3,p_4,\lambda_3,\lambda_4) &= D^{\mu\nu}_W(p_{34})\bar{u}_3(p_3,\lambda_3)\gamma_\nu g_W\\
&\quad\times P_- v_4(p_4,\lambda_4),\\
\varepsilon^\mu_{W^-}(p_5,p_6,\lambda_5,\lambda_6) &= D^{\mu\nu}_W(p_{56})\bar{u}_5(p_5,\lambda_5)\gamma_\nu g_W\\
&\quad\times P_- v_6(p_6,\lambda_6),
\end{aligned} \quad (20)$$

where we have introduced the shorthand notation $p_{12} = p_1+p_2$, $p_{34} = p_3+p_4$ and $p_{56} = p_5+p_6$; $g_{\gamma e}, g^{(\pm)}_{Ze}$ and g_W are the standard model couplings. We use constant widths for the massive gauge bosons. They are introduced through the complex mass parameters $M_V^2 = m_V^2 - \mathrm{i}m_V\Gamma_V$ in the propagators $D_V^{\mu\nu}, V = W, Z$. However, we keep a real value of the electroweak mixing parameter $\sin\theta_{\mathrm{W}}$. This simple prescription preserves the electromagnetic gauge invariance, also for the nonzero fermion masses. This has been checked analytically and confirmed by the numerical calculation. We would like to stress at this point that this result is obtained with two independent widths Γ_W and Γ_Z which violate the $SU(2)$ gauge invariance. This finding seems to contradict the discussion of this issue in [13]. The resulting violation of the high energy unitarity cancellations for $e^+e^- \to 4f$ is suppressed by the factor $\Gamma_W M_W/s$. A comparison of different gauge boson width prescriptions performed in [6] and [12] shows that our simple prescription is satisfactory as far as the experimental precision of LEP2 and future linacs is concerned.

Using polarization vectors (20) we can express the helicity amplitudes of reaction (19) corresponding to the diagrams of Fig. 1 in terms of the functions defined in (14), (16) and (18):

$$\begin{aligned}
M_1 &= F_3\big(\bar{v}_1, 0, g_W\varepsilon^-_{W^+}, p_2^+ - p_{56}^+, p_2^- - p_{56}^-, 0,\\
&\qquad g_W\varepsilon^-_{W^-}, u_2\big),\\
M_2 + M_3 &= E_3\big(p_{56}, \varepsilon_{W^-}, p_{34}, \varepsilon_{W^+}, p_{12}, g_{WW\gamma}\varepsilon_\gamma\\
&\qquad + g_{WWZ}\varepsilon_Z\big),\\
M_4 + M_5 &= F_3\big(\bar{u}_3, g_{\gamma u}\varepsilon^+_\gamma + g^{(+)}_{Zu}\varepsilon^+_Z, g_{\gamma u}\varepsilon^-_\gamma + g^{(-)}_{Zu}\varepsilon^-_Z,\\
&\qquad p_3^+ - p_{12}^+, p_3^- - p_{12}^-, m_3, 0, g_W\varepsilon^-_{W^-}, v_4\big),\\
M_6 + M_7 &= F_3\big(\bar{u}_3, 0, g_W\varepsilon^-_{W^-}, p_{12}^+ - p_4^+, p_{12}^- - p_4^-,\\
&\qquad m_4, g_{\gamma d}\varepsilon^+_\gamma + g^{(+)}_{Zd}\varepsilon^+_Z, g_{\gamma d}\varepsilon^-_\gamma + g^{(-)}_{Zd}\varepsilon^-_Z, v_4\big),\\
M_8 + M_9 &= F_3\big(\bar{u}_5, g_{\gamma\mu}\varepsilon^+_\gamma + g^{(+)}_{Z\mu}\varepsilon^+_Z, g_{\gamma\mu}\varepsilon^-_\gamma + g^{(-)}_{Z\mu}\varepsilon^-_Z,\\
&\qquad p_5^+ - p_{12}^+, p_5^- - p_{12}^-, m_5, 0, g_W\varepsilon^-_{W^+}, v_6\big),\\
M_{10} &= F_3\big(\bar{u}_5, 0, g_W\varepsilon^-_{W^+}, p_{12}^+ - p_6^+, p_{12}^- - p_6^-,\\
&\qquad 0, 0, g_{Z\nu}\varepsilon^-_Z, v_4\big),
\end{aligned} \quad (21)$$

where we have used the shorthand notation $v_i = v_i(\boldsymbol{p}_i,\lambda_i)$, $i = 1,4,6$, $u_j = u_j(\boldsymbol{p}_j,\lambda_j)$, $j = 2,3,5$ for the spinors which are defined according to (5). The standard model couplings of (20) and (21) are defined in terms of the electric charge e and the electroweak mixing parameter $\sin^2\theta_{\mathrm{W}}$.

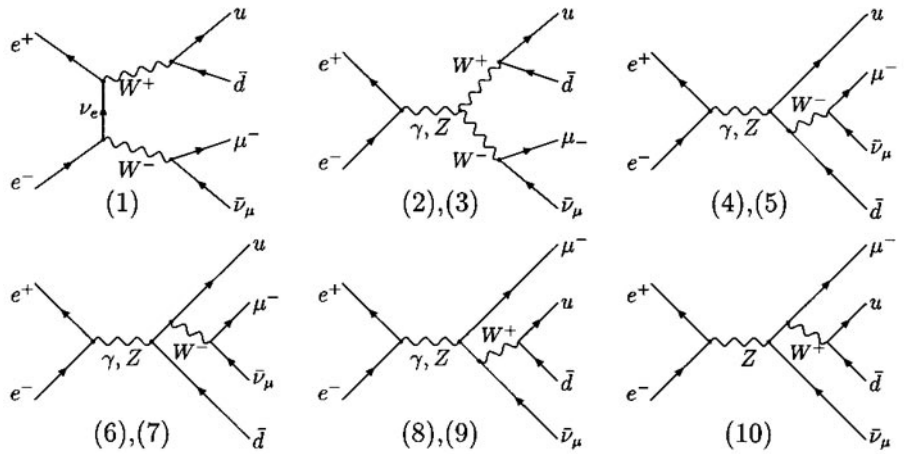

Fig. 1. The Feynman diagrams of reaction (19)

By comparing (21) with Fig. 1 one observes that the diagrams which differ only by the replacement of the photon and Z propagators can be calculated simultaneously. This is one of the advantages of the method presented.

Now the modulus squared of the spin averaged matrix element of the reaction (19) can easily be computed numerically.

The matrix element of the bremsstrahlung reaction

$$e^+(p_1)+ e^- (p_2) \to u(p_3) + \bar{d}(p_4) + \mu^-(p_5) + \bar{\nu}_\mu(p_6) + \gamma(p_7), \tag{22}$$

where the particle four-momenta are indicated in parenthesis is calculated in the same way. The 71 Feynman diagrams of the process (22) can be obtained from those of Fig. 1 by attaching an external photon line to each charged particle as well as to the triple gauge boson vertex. We again neglect the Higgs boson contribution.

In the soft photon limit, $|\boldsymbol{p}_7| < \omega$, the matrix element of reaction (22) takes the simple factorized form

$$\begin{aligned} M_\gamma\ & (p_1,p_2,p_3,p_4,p_5,p_6,p_7,\lambda_1,\lambda_2,\lambda_3,\lambda_4, \\ & \lambda_5,\lambda_6,\lambda_7)|_{|\boldsymbol{p}_7|<\omega} \\ = & -\left(g_{\gamma l}\frac{p_1^\mu}{p_1\cdot p_7} - g_{\gamma l}\frac{p_2^\mu}{p_2\cdot p_7} + g_{\gamma u}\frac{p_3^\mu}{p_3\cdot p_7}\right. \\ - & \left. g_{\gamma d}\frac{p_4^\mu}{p_4\cdot p_7} + g_{\gamma l}\frac{p_5^\mu}{p_5\cdot p_7}\right)\varepsilon_\mu(p_7,\lambda_7) \\ \times & \ M_0(p_1,p_2,p_3,p_4,p_5,p_6,\lambda_1,\lambda_2,\lambda_3,\lambda_4,\lambda_5,\lambda_6), \end{aligned} \tag{23}$$

where M_0 is the matrix element of reaction (19) and the photon–fermion couplings are given by $g_{\gamma l} = e$, $g_{\gamma u} = 2/3e$ and $g_{\gamma d} = -e/3$.

4 The phase space integration

The phase space integration is performed with the Monte Carlo integration routine VEGAS [15]. We integrate out the dependence on the azimuthal angle related to the rotational symmetry with respect to the beam axis. This symmetry is satisfied as long as we do not consider transversely polarized initial beams. Thus, the number of integrations is reduced from 8 to 7 and from 11 to 10 for reactions (19) and (22), respectively.

The 7 dimensional phase space element of the reaction (19) is parametrized by

$$\begin{aligned} \mathrm{d}^7 Lips = (2\pi)^{-7}\frac{\lambda^{1/2}(s,s_{34},s_{56})}{8s}\frac{\lambda^{1/2}(s_{34},m_3^2,m_4^2)}{8s_{34}} \\ \times\frac{\lambda^{1/2}(s_{56},m_5^2,m_6^2)}{8s_{56}}\mathrm{d}s_{34}\mathrm{d}s_{56}\mathrm{d}\cos\theta\mathrm{d}\Omega_3\mathrm{d}\Omega_5, \end{aligned} \tag{24}$$

where $s = (p_1+p_2)^2$, $s_{34} = (p_3+p_4)^2$, $s_{56} = (p_5+p_6)^2$, θ is an angle between the momenta $\boldsymbol{p}_3 + \boldsymbol{p}_4$ and the z axis of the c.m. system which is directed along the positron momentum $\boldsymbol{p}_1$. $\mathrm{d}\Omega_3 = \mathrm{d}\cos\theta_3\mathrm{d}\phi_3$ ($\mathrm{d}\Omega_5 = \mathrm{d}\cos\theta_5\mathrm{d}\phi_5$) is the solid angle element of $\boldsymbol{p}_3$ ($\boldsymbol{p}_5$) in the respective c.m. frame where $\boldsymbol{p}_3 + \boldsymbol{p}_4 = 0$ ($\boldsymbol{p}_5 + \boldsymbol{p}_6 = 0$).

The integration limits in the invariants s_{34} and s_{56} of (24) are given by

$$(m_3+m_4)^2 \le s_{34} \le (\sqrt{s}-m_5-m_6)^2, \tag{25}$$

$$(m_5+m_6)^2 \le s_{56} \le (\sqrt{s}-\sqrt{s_{34}})^2 \tag{26}$$

and the spherical angles vary in the full range, i.e.

$$\begin{aligned} -1 \le \cos\theta \le 1, \\ 0 \le \Omega_i \le 4\pi, \quad i = 3,5. \end{aligned} \tag{27}$$

The 10 dimensional phase space element of the reaction (22) is parametrized in different ways dependent on whether we want to account for the peaking related to the photon emission from the initial or final state fermions. In order to deal with the initial state radiation peaking we parametrize the phase space by

$$\begin{aligned} \mathrm{d}^{10} Lips = (2\pi)^{-10}\frac{E_7}{2}\frac{\lambda^{1/2}(s',s_{34},s_{56})}{8s'}\frac{\lambda^{1/2}(s_{34},m_3^2,m_4^2)}{8s_{34}} \\ \times\frac{\lambda^{1/2}(s_{56},m_5^2,m_6^2)}{8s_{56}}\mathrm{d}E_7\mathrm{d}\Omega_7\mathrm{d}s_{34}\mathrm{d}s_{56}\mathrm{d}\cos\theta_{34}\mathrm{d}\Omega_3\mathrm{d}\Omega_5, \end{aligned} \tag{28}$$

where $s' = (p_1+p_2-p_7)^2$. The photon variables, the energy E_7, and the solid angle Ω_7, are defined in the frame where $\boldsymbol{p}_1 + \boldsymbol{p}_2 - \boldsymbol{p}_7 = 0$. The polar angle θ_{34} of the momentum vector $\boldsymbol{p}_3+\boldsymbol{p}_4$ with respect to the positron beam is defined in the same frame. The invariant masses s_{34}, s_{56} and solid angles Ω_3, Ω_5 are defined as in (24).

The integration limits in the photon energy E_7 and in the invariants s_{34}, s_{56} of (28) read

$$E_{\rm cut} \le E_7 \le \frac{s-(m_3+m_4+m_5+m_6)^2}{2\sqrt{s}}, \quad (29)$$

$$(m_3+m_4)^2 \le s_{34} \le (\sqrt{s'}-m_5-m_6)^2, \quad (30)$$

$$(m_5+m_6)^2 \le s_{56} \le (\sqrt{s'}-\sqrt{s_{34}})^2, \quad (31)$$

where $E_{\rm cut}$ is the minimum hard photon energy to be detected and $s' = \sqrt{s}(\sqrt{s}-2E_7)$. The spherical angles of (28) vary in the full range, as in (27).

On the other hand, the radiation off the final state $\bar{d}$ quark is dealt with in another parametrization:

$$\mathrm{d}^{10}\ Lips = (2\pi)^{-10}\frac{\lambda^{1/2}(s,s_{347},s_{56})}{8s}\frac{\lambda^{1/2}(s_{56},m_5^2,m_6^2)}{8s_{56}} \times\frac{1}{8}\mathrm{d}s_{347}\mathrm{d}s_{56}\mathrm{d}\cos\theta_{347}\mathrm{d}E_3\mathrm{d}E_7\mathrm{d}\Omega_3\mathrm{d}\phi_{37}\mathrm{d}\Omega_5, \quad (32)$$

where the polar angle θ_{347} of the momentum $\boldsymbol{p}_3+\mathbf{p}_4+\boldsymbol{p}_7$ is defined in the c.m.s.; the energy E_3 and the spherical angle Ω_3 of the u quark, the photon energy E_7 and the azimuthal angle ϕ_{37} between the u quark and the γ are defined in the relative c.m.s. of u and $\bar{d}$ quarks and the photon; the spherical angle Ω_5 is defined in the c.m.s. of the μ^- and $\bar{\nu}_\mu$.

The integration limits are now specified by

$$(m_3+m_4)^2 \le s_{347} \le (\sqrt{s}-m_5-m_6)^2, \quad (33)$$

$$(m_5+m_6)^2 \le s_{56} \le (\sqrt{s}-\sqrt{s_{347}})^2, \quad (34)$$

$$m_3 \le E_3 \le \left[m_3^2+\lambda(s,m_3^2,m_4^2(1+E_{\rm cut}/E_4^{\rm max}))/(4s)\right]^{1/2}, \quad (35)$$

$$E'_{\rm cut} \le E_7 \le \frac{(\sqrt{s}-E_3)^2-E_3^2+m_3^2-m_4^2}{2(\sqrt{s}-E_3-|\boldsymbol{p}_3|)}, \quad (36)$$

where $E'_{\rm cut}$ is the photon energy cut transformed to the c.m.s. of $u\bar{d}\gamma$ and $E_4^{\rm max} = \left[m_4^2+\ \lambda(s,m_3^2,m_4^2)/(4s)\right]$ is the maximum of the $\bar{d}$ quark energy. We have neglected $E_{\rm cut}$ on the left hand side of (33) and $E'_{\rm cut}$ in $E_4^{\rm max}$, which simplifies the corresponding analytic expressions. The correct phase space boundaries are then restored by checking the condition $E_7 \ge E_{\rm cut}$ in the c.m.s. numerically. The spherical angles of (32) vary again in the full range.

The phase space parametrization convenient for the description of the photon radiation off the u quark or μ^- is obtained from (32) by a permutation of the final state momenta.

In order to improve the convergence of the phase space integration we perform the following mappings. The Breit–Wigner shape of the $W^\pm$ resonances is taken into account by the mapping

$$s_W = \Gamma_W m_W \tan\left(\frac{\Gamma_W m_W}{N_W}x+\psi_{\rm min}\right)+m_W^2, \quad (37)$$

where N_W is the normalization factor, $N_W = \Gamma_W m_W /(\psi_{\rm max}-\psi_{\rm min})$, with $\psi_{\rm min} = \arctan(s_W^{\rm min}-m_W^2)/(\Gamma_W m_W)$ and $\psi_{\rm max} = \arctan(s_W^{\rm max}-m_W^2)/(\Gamma_W m_W)$. The $1/t$ pole due to the neutrino exchange diagram (1) of Fig. 1 is mapped by transforming the polar angle of the virtual W^+ boson with respect to the positron beam $\theta_{\rm W}$ according to

$$\cos\theta_{\rm W} = (1-(1+\beta_W)r_W^{-x})/\beta_W, \quad (38)$$

where β_W stands for for the velocity of the W^+ boson and $r_W = (1+\beta_W)/(1-\beta_W)$.

The $\sim 1/E_7$ peaking of the bremsstrahlung photon spectrum is eliminated by the mapping

$$E_7 = E_7^{\rm min}\left(E_7^{\rm max}/E_7^{\rm min}\right)^x, \quad (39)$$

where $E_7^{\rm min}$ and $E_7^{\rm max}$ are the lower and upper limit of the photon energy. The strong collinear peaking behavior of the squared matrix element of reaction (22) corresponding to the radiation off the initial state positron $\sim 1/(1-\beta\cos\theta_7)$ is eliminated by the mapping

$$\cos\theta_7 = \frac{1}{\beta_e}\left(1-(1+\beta_e)/r_e^x\right) \quad (40)$$

with $r_e = (1+\beta_e)/(1-\beta_e)$ and $\beta_e = \sqrt{1-4m_e^2/s}$ being the velocity of the electron in the c.m. system. Similarly, the collinear peaking related to the radiation off the initial state electron $\sim 1/(1+\beta\cos\theta_7)$ is dealt with the mapping

$$\cos\theta_7 = \frac{1}{\beta_e}\left((1-\beta_e)r_e^x-1\right). \quad (41)$$

Finally, the collinear and soft photon peaking corresponding to radiation off the final state fermion must be mapped away, e.g. for the $\bar{d}$ quark, $1/(p_4\cdot p_7) \sim 1/(C_3-E_3)$ is eliminated by the mapping

$$E_3 = C_3-(C_3-m_3)\left(\frac{C_3-E_3^{\rm max}}{C_3-m_3}\right)^x, \quad (42)$$

where $C_3 = \sqrt{s_{347}}/2+(m_3^2-m_4^2)/(2\sqrt{s_{347}})$. In (37–42), x denotes a random variable uniformly distributed in the interval $[0,1]$.

The phase space parametrizations (28) and (32) together with the mappings (37–42) are implemented in a single multichannel Monte Carlo program in a way described in [16]. We use five different channels corresponding to the photon radiation off each charged particle with equal weights.

In the soft photon limit, we can perform the integration over the photon phase space analytically:

$$|\mathrm{d}\sigma_\gamma|_{|\boldsymbol{p}_7|<\omega} = -\frac{1}{(2\pi)^3}\int_{|\boldsymbol{p}_7|<\omega}\frac{\mathrm{d}^3p_7}{2E_7}\left(g_{\gamma l}\frac{p_1}{p_1\cdot p_7} - g_{\gamma l}\frac{p_2}{p_2\cdot p_7}+g_{\gamma u}\frac{p_3}{p_3\cdot p_7}-g_{\gamma d}\frac{p_4}{p_4\cdot p_7}+g_{\gamma l}\frac{p_5}{p_5\cdot p_7}\right)^2\mathrm{d}\sigma_0 = -\sum_{i,j=1}^{5}g_{\gamma i}g_{\gamma j}I_{ij}^{\omega}. \quad (43)$$

Table 1. Born cross sections in pb (no cuts)

$E_{\rm cm}$ GeV	$\sigma_0^{\rm all}$	$\sigma_0^{\rm all}$ [16]
162.5	0.2685(0.4)	0.2688(3)
180.0	0.6612(0.9)	0.6616(7)
189.0	0.7037(1.0)	0.7044(8)
500.0	0.2810(0.5)	0.2817(5)
1000.0	0.1078(0.3)	0.1079(2)
2000.0	0.03736(1.2)	0.03748(8)
10000.0	0.002563(3)	0.002578(16)

Table 2. Cross sections[3] in fb with the "canonical" cuts (46)

$E_{\rm cm}$ GeV	σ_0	σ_0 [12]	σ_γ	σ_γ [12]
189.0	703.1(1)	703.5(3)	223.2(8)	224.0(4)
500.0	237.4(1)	237.4(1)	83.3(6)	83.4(3)
2000.0	13.96(1)	13.99(2)	7.05(8)	6.98(5)
10000.0	0.625(1)	0.624(3)	0.459(9)	0.457(6)

The bremsstrahlung integrals I_{ij}^{ω}, which are defined by

$$I_{ij}^{\omega} = \frac{1}{(2\pi)^3} \int_{|\boldsymbol{p}_7|<\omega} \frac{\mathrm{d}^3 p_7}{2E_7} \frac{p_i \cdot p_j}{(p_i \cdot p_7)(p_j \cdot p_7)}, \qquad (44)$$

for $i \neq j$ may be found in Sect. 7 of [17]. For $i = j$ we have

$$I_{ii}^{\omega} = \ln \frac{2\omega}{m_\gamma} - \frac{1}{\beta_i} \ln \frac{1+\beta_i}{1-\beta_i}, \qquad (45)$$

where β_i is the velocity of the radiating particle in the c.m.s. and m_γ denotes a fictitious mass of the photon.

5 Numerical results

We now present our results for the Born cross section $e^+e^- \to u\bar{d}\mu^-\bar{\nu}_\mu$ and the corresponding hard bremsstrahlung process. We use the following physical parameters: the gauge boson masses and widths are $m_W = 80.23\,\mathrm{GeV}$, $\Gamma_W = 2.085\,\mathrm{GeV}$, $m_Z = 91.1888\,\mathrm{GeV}$, $\Gamma_Z = 2.4974\,\mathrm{GeV}$, the fermion masses are $m_e = 0.51099906\,\mathrm{MeV}$, $m_\mu = 105.658389\,\mathrm{MeV}$, $m_\tau = 1777.05\,\mathrm{MeV}$, $m_u = 5\,\mathrm{MeV}$, $m_d = 10\,\mathrm{MeV}$, $m_s = 170\,\mathrm{MeV}$, $m_c = 1.3\,\mathrm{GeV}$. The electroweak standard model couplings are parametrized by $\alpha_W = 1/128.07$ and by the electroweak mixing parameter $\sin^2\theta_{\rm W} = 0.22591$. The couplings of the bremsstrahlung photon are parametrized by $\alpha = 1/137.0359895$ which means in practice that we multiply the matrix element squared by the ratio α/α_W.

Our results have been thoroughly tested and checked against other calculations. The matrix elements have been checked against MADGRAPH [18]. Moreover, as we already mentioned in Sect. 3, we have checked the electromagnetic gauge invariance of the matrix element of the bremsstrahlung process both analytically and numerically. The phase space integrals have been checked against their asymptotic limits which have been obtained analytically.

[3] Here we adopt the parameters of [12]: $m_W = 80.26\,\mathrm{GeV}$, $\Gamma_W = 2.05\,\mathrm{GeV}$, $m_Z = 91.1884\,\mathrm{GeV}$, $\Gamma_Z = 2.46\,\mathrm{GeV}$, $\alpha = \alpha_W = 1/128.89$ and $\sin^2\theta_{\rm W} = 1 - m_W^2/m_Z^2$. The fermion masses play no role in the presence of the cuts.

Table 3. Cut independence of $\sigma_\gamma = \sigma_s + \sigma_h$ The photon mass is $m_\gamma = 10^{-6}\,\mathrm{GeV}$

$E_{\rm cm}$(GeV)	ω (GeV)	σ_s (fb)	σ_h (fb)	$\sigma_s + \sigma_h$ (fb)
189	0.001	202.6(2)	1083(1)	1285
	0.1	712.2(5)	572.8(6)	1285
	1.0	967.0(7)	319.3(3)	1286
500	0.001	42.53(4)	528.3(1.0)	570.8
	0.1	247.3(2)	322.7(6)	570.0
	1.0	349.7(3)	220.4(4)	570.0
2000	0.1	26.73(4)	55.8(3)	82.5
	1.0	40.75(8)	42.4(3)	83.1
10000	0.1	1.302(5)	4.85(6)	6.15
	1.0	2.265(8)	3.84(6)	6.10

The total cross sections in the Born approximation are compared against EXCALIBUR [16] in Table 1, with no cuts applied. In Table 2, we compare the Born cross sections σ_0 and the corresponding hard bremsstrahlung cross sections σ_γ with the results of [12] in the so-called constant width scheme and with phase space integration restricted by the "canonical" cuts. Let l, q, γ, and "beam" denote charged leptons, quarks, photons, and the beam (electrons or positrons), respectively, and $\theta(i,j)$ the angles between the particles i and j in the c.m. system. Furthermore, $m(q,q')$ denotes the invariant mass of a quark pair qq'. The "canonical" cuts then read

$$\begin{aligned} &\theta(l,\mathrm{beam}) > 10^\circ, \quad \theta(l,l') > 5^\circ, \quad \theta(l,q) > 5^\circ, \\ &\theta(\gamma,\mathrm{beam}) > 1^\circ, \quad \theta(\gamma,l) > 5^\circ, \quad \theta(\gamma,q) > 5^\circ, \\ &E_\gamma > 0.1\,\mathrm{GeV}, \quad E_l > 1\,\mathrm{GeV}, \quad E_q > 3\,\mathrm{GeV}, \\ &m(q,q') > 5\,\mathrm{GeV}\,. \end{aligned} \qquad (46)$$

Except for the additional angular cut between the charged leptons, which is irrelevant for the reactions considered here anyway, these cuts which exclude all collinear and infrared singularities coincide with those defined in [1]. Another test, which is very sensitive to the treatment of the infrared and collinear singularities, is obtained by splitting the photon radiation cross section (22) into a soft and a hard part $\sigma_\gamma = \sigma_{\rm s} + \sigma_{\rm h}$ and checking the independence of the separation cut. The soft part includes the photons with $E_\gamma < \omega$ and is given by (43). The hard part then includes all photons with energies $E_\gamma > \omega$. Furthermore, the total "inclusive" cross section is $\sigma = \sigma_0 + \sigma_{\rm s} + \sigma_{\rm h}$. Since we have not yet included the infrared (IR) singular virtual one-loop corrections, $\sigma_{\rm s}$ only exists when it is IR regularized in some way. Here we have chosen a small photon mass $m_\gamma = 10^{-6}\,\mathrm{GeV}$. We demonstrate the cut

Table 4. Mass dependence of cross sections (in fb; without cuts, except for $E_\gamma > 0.1\,\mathrm{GeV}$) for different final states

E_{cm} GeV	$\sigma_0(u\bar{d}\mu^-\bar{\nu}_\mu)$	$\sigma_0(c\bar{s}\mu^-\bar{\nu}_\mu)$	$\sigma_0(u\bar{d}\tau^-\bar{\nu}_\tau)$	$\sigma_\gamma(u\bar{d}\mu^-\bar{\nu}_\mu)$	$\sigma_\gamma(c\bar{s}\mu^-\bar{\nu}_\mu)$	$\sigma_\gamma(u\bar{d}\tau^-\bar{\nu}_\tau)$
189.0	704.1(4)	703.8(4)	703.5(4)	573.4(4)	525.2(4)	522.6(4)
360.0	422.0(2)	421.8(2)	421.5(2)	448.5(4)	418.4(4)	414.1(4)
500.0	281.0(2)	280.9(2)	281.0(2)	322.8(4)	302.0(4)	298.1(3)
2000.0	37.33(4)	37.32(4)	37.32(4)	56.48(27)	53.19(25)	52.67(13)

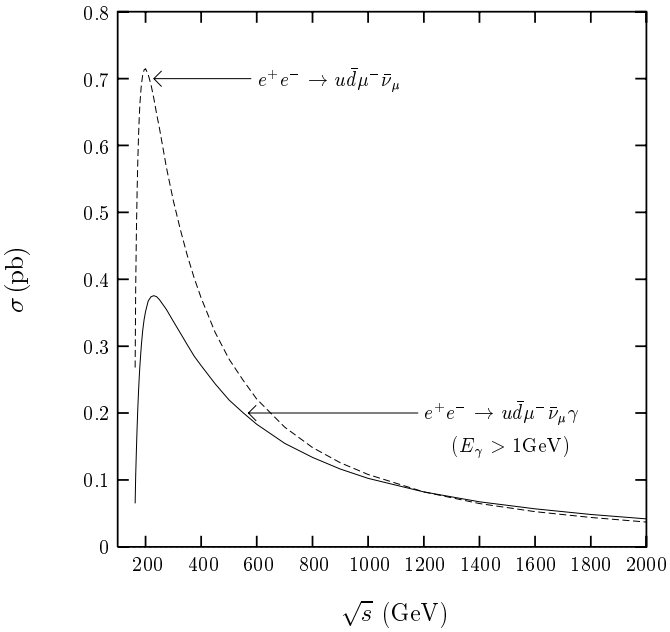

Fig. 2. The energy dependence of the total cross sections of reactions (19) and (22)

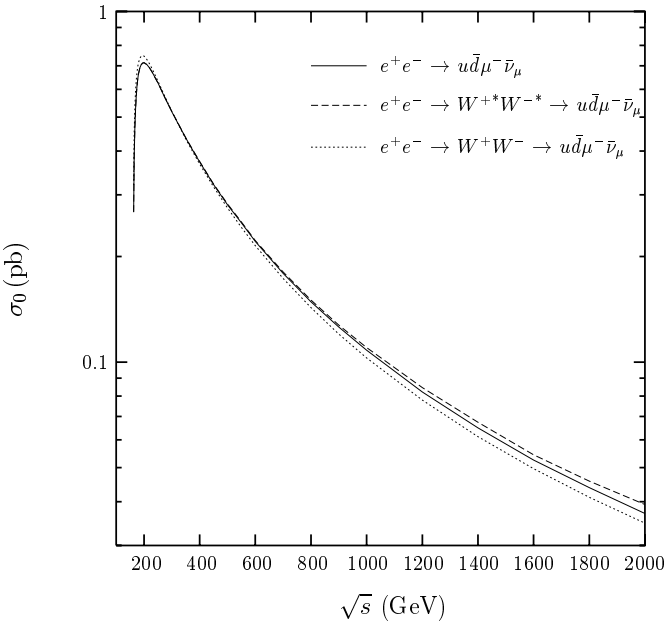

Fig. 3. Lowest order cross sections obtained by including (**i**) all diagrams, (**ii**) only diagrams with W^*W^* intermediate states and (**iii**) production and decay of on-shell W pairs (zero width approximation)

(ω) independence of the soft–hard splitting in Table 3. It is a measure of the numerical stability of our calculation as well as a test for the validity of the factorization into a radiation factor times the non-radiative cross section (43).

Finally, in Table 4 we illustrate the mass dependence of the cross sections of related channels. The replacements $ud \to cs$ and $\mu \to \tau$ lead to comparable effects. While the Born cross sections remain practically unchanged the hard bremsstrahlung cross section, for the energy cut $E_\gamma > 0.1\,\mathrm{GeV}$, changes by about -9% (189 GeV) to about -6% (2 TeV).

The energy dependence of the total cross sections σ_0 and σ_γ of reactions $e^+e^- \to u\bar{d}\mu^-\bar{\nu}_\mu$ and $e^+e^- \to u\bar{d}\mu^-\bar{\nu}_\mu\,\gamma$, respectively, is shown in Fig. 2. The hard bremsstrahlung cross section has been calculated with the photon energy cut of $E_\gamma = 1\,\mathrm{GeV}$.

At this point we would like to address the problem of $SU(2)$ gauge-symmetry violation caused by introducing the constant widths Γ_W and Γ_Z in a more quantitative way. For this purpose, in Fig. 3, we compare the $e^+e^- \to u\bar{d}\mu^-\bar{\nu}_\mu$ cross sections obtained when

(i) including all diagrams,
(ii) including only WW diagrams and
(iii) assuming the creation of an on-shell $W^\pm$ pair and the subsequent decays $W^- \to \mu^-\bar{\nu}_\mu$ and $W^+ \to u\bar{d}$ ($e^+e^- \to W^+W^- \to u\bar{d}\mu^-\bar{\nu}_\mu$).

Cases (**i**) and (**ii**) for the corresponding bremsstrahlung reaction with the photon energy cut $E_\gamma > 1\,\mathrm{GeV}$ are plotted in Fig. 4. Although the constant width prescription violates unitarity by spoiling the gauge cancellations in both cases (**i**) and (**ii**), the unitarity violation is much stronger in case (**ii**) where we have neglected the non double-resonant diagrams. In case (**i**) the effect is practically negligible, at least in the energy range presented in Fig. 3. This observation relies on the comparison with the results of [12]. Our results which were calculated in the linear gauge agree within statistical errors with those of [12] which were obtained in a nonlinear gauge in the so-called complex mass scheme that preserves the Ward identities. In Figs. 3 and 4 we observe that the double-resonant approximation provides a good approximation of the complete calculation for c.m. energies from thresh-

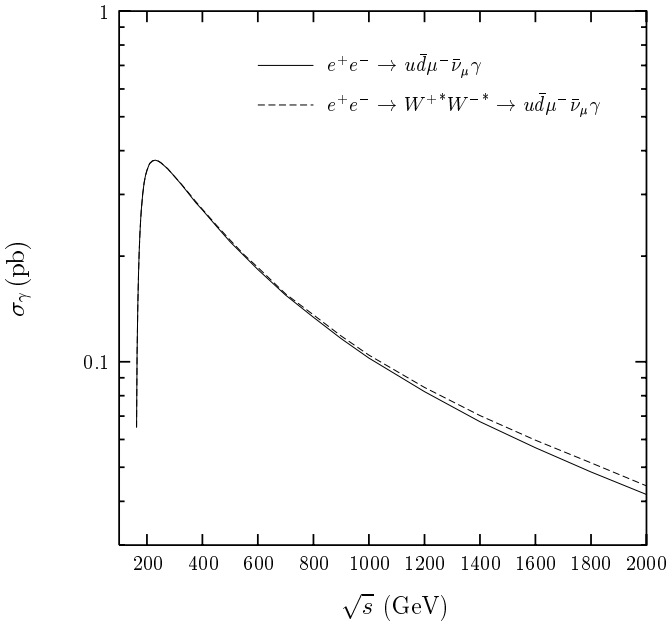

Fig. 4. Bremsstrahlung cross sections for $E_\gamma > 1\,\mathrm{GeV}$ obtained by including (**i**) all diagrams, (**ii**) only diagrams with W^*W^* intermediate states

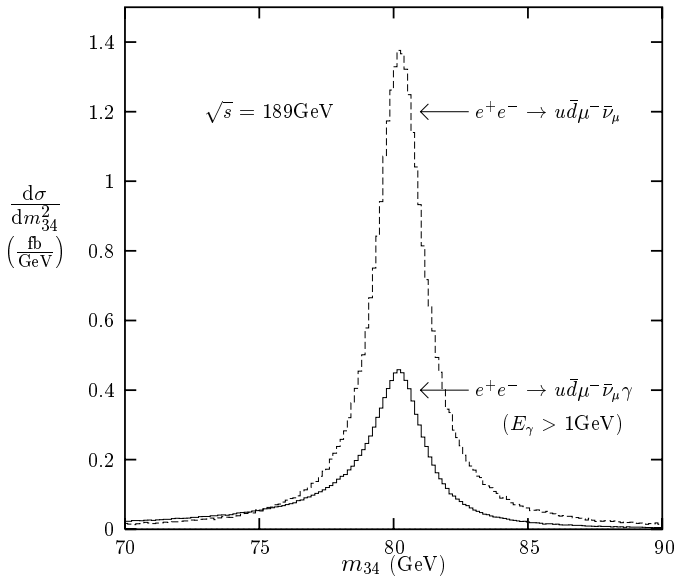

Fig. 6. The differential cross section $\mathrm{d}\sigma/\mathrm{d}m_{34}^2$ at $s^{1/2} = 189\,\mathrm{GeV}$ versus the invariant mass of the $u\bar{d}$ pair m_{34}. The upper curve corresponds to the tree level reaction (19) and the lower curve to the bremsstrahlung reaction (22) with $E_\gamma > 1\,\mathrm{GeV}$

old up to about 250 GeV. However, it already deviates by 0.5% (more than 1% for reaction (22)) at $s^{1/2} = 500\,\mathrm{GeV}$ and by about 2% at $s^{1/2} = 1\,\mathrm{TeV}$. On the other hand, we see that the zero width approximation, which is gauge invariant by definition, deviates from the complete tree level calculation by almost 18% at $s^{1/2} = 165\,\mathrm{GeV}$, by 4.3% at $s^{1/2} = 200\,\mathrm{GeV}$ and by -4.5% at $s^{1/2} = 1\,\mathrm{TeV}$.

The photon spectra at $s^{1/2} = 189\,\mathrm{GeV}$ and $s^{1/2} = 500\,\mathrm{GeV}$ are shown in Fig. 5. We see that the spectra are relatively soft, with a substantial fraction of events having photon energies of $O(\Gamma_W)$. A bump of the 189 GeV spectrum at $E_\gamma \sim 25\,\mathrm{GeV}$ reflects the W pair production threshold. We finally plot $\mathrm{d}\sigma/\mathrm{d}m_{34}^2$ at $s^{1/2} = 189\,\mathrm{GeV}$ as a function of the invariant mass of the $u\bar{d}$ pair m_{34} in Fig. 6.

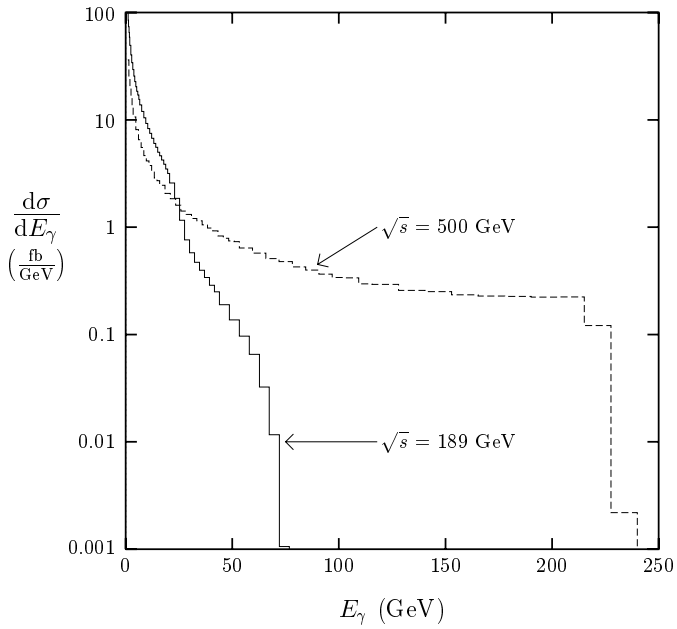

Fig. 5. The photon spectra at $s^{1/2} = 189\,\mathrm{GeV}$ and $s^{1/2} = 500\,\mathrm{GeV}$

6 Conclusions and outlook

We have presented an efficient method for calculating photon radiation cross sections for massive fermions. For the collinear region such finite mass calculations provide important tests for Monte Carlo generators which work with massless fermions. We have studied a complete signal plus background process with all possible real photon emission diagrams for the interesting channel $e^+e^- \to u\bar{d}\mu^-\bar{\nu}_\mu$. This channel is particularly suited for a detailed investigation of effects related to final state photon emission, since the muons appear well separated from photons in the detectors. In particular it seems to be interesting to study the influence of final state radiation on the W mass measurement via this channel. In addition, at a high luminosity linear collider, like TESLA, one could study the quark mass effects due to the different quark flavor channels in $e^+e^- \to \mu^-\bar{\nu}_\mu$ + hadrons. Of particular interest would be a detailed investigation of the single top production channel $e^+e^- \to t\bar{b}\mu^-\bar{\nu}_\mu$ which will be discussed in a forthcoming paper.

Acknowledgements. One of us (K.K.) would like to thank H. Czyż and J. Sładkowski for discussions. Furthermore, we thank

T. Riemann for helpful discussions and for carefully reading the manuscript

References

1. D. Bardin et al., Event generators for WW physics, in Physics at LEP2, CERN 96-01 (1996), edited by G. Altarelli, T. Sjöstrand, F. Zwirner, vol. 2, pp. 3-353
2. D. Karlen, Experimental Status of the Standard Model, in Proceedings of 29th International Conference on High-Energy Physics (ICHEP 98), 23–29 July 1998, Vancouver, Canada
3. M. Böhm et al., Nucl. Phys. B **304**, 463 (1988); J. Fleischer, F. Jegerlehner, M. Zrałek, Z. Phys. C **42**, 409 (1989)
4. K. Kołodziej, M. Zrałek, Phys. Rev. D **43**, 3619 (1991)
5. W. Beenakker, K. Kołodziej, T. Sack, Phys. Lett. B **258**, 469 (1991); W. Beenakker, F.A. Berends, T. Sack, Nucl. Phys. B **367**, 287 (1991); J. Fleischer, K. Kołodziej, F. Jegerlehner, Phys. Rev. D **47**, 830 (1993)
6. S. Dittmaier, CERN-TH/98-336, hep-ph/9811434
7. A. Vicini, Acta Phys. Pol. B **29**, 2847 (1998)
8. A. Aeppli, D. Wyler, Phys. Lett. B **262**, 125 (1991); A. Aeppli, Doctoral thesis, Universität Zürich (1992)
9. G.J. van Oldenborgh, P.J. Franzini, A. Borrelli, Comput. Phys. Commun. **83**, 14 (1994)
10. J. Fujimoto, et al., Nucl. Phys. (Proc. Suppl.) 37B (1994) 169
11. F. Caravaglios, M. Moretti, Z. Phys. C **74**, 291 (1997)
12. A. Denner, S. Dittmaier, M. Roth, D. Wackeroth, BI-TP 99/10, PSI-PR-99-12, hep-ph/9904472
13. W. Beenakker, A. Denner, Acta Phys. Pol. B **29**, 2821 (1998)
14. W. Beenakker, F.A. Berends, A.P. Chapovsky, Phys. Lett. B **435**, 233 (1998)
15. G.P. Lepage, J. Comp. Phys. **27**, 192 (1978)
16. F.A. Berends, R. Pittau, R. Kleiss, Nucl. Phys. B **424**, 308 (1994); Comput. Phys. Commun. **85**, 437 (1995)
17. G. 't Hooft, M. Veltman, Nucl. Phys. B **153**, 365 (1979)
18. T. Stelzer, W.F. Long, Comput. Phys. Commun. **81**, 357 (1994); E. Murayama, I. Watanabe, K. Hagiwara, KEK report 91–11, 1992